BIOCHEMISTRY
including biophysical chemistry & molecular biology

Article

pubs.acs.org/biochemistry

The Diheme Cytochrome *c* Peroxidase from *Shewanella oneidensis* Requires Reductive Activation

Gökçe Su Pulcu,[†] Katherine E. Frato,[†] Rupal Gupta,[‡] Hao-Ru Hsu,[†] George A. Levine,[†] Michael P. Hendrich,[‡] and Sean J. Elliott*[,†]

[†]Department of Chemistry, Boston University, 590 Commonwealth Avenue, Boston, Massachusetts 02215, United States

[‡]Department of Chemistry, Carnegie Mellon University, Pittsburgh, Pennsylvania 15213, United States

Supporting Information

ABSTRACT: We report the characterization of the diheme cytochrome *c* peroxidase (CcP) from *Shewanella oneidensis* (*So*) using UV−visible absorbance, electron paramagnetic resonance spectroscopy, and Michaelis−Menten kinetics. While sequence alignment with other bacterial diheme cytochrome *c* peroxidases suggests that *So* CcP may be active in the as-isolated state, we find that *So* CcP requires reductive activation for full activity, similar to the case for the canonical *Pseudomonas* type of bacterial CcP enzyme. Peroxide turnover initiated with oxidized *So* CcP shows a distinct lag phase, which we interpret as reductive activation in situ. A simple kinetic model is sufficient to recapitulate the lag-phase behavior of the progress curves and separate the contributions of reductive activation and peroxide turnover. The rates of catalysis and activation differ between MBP fusion and tag-free *So* CcP and also depend on the identity of the electron donor. Combined with Michaelis−Menten analysis, these data suggest that *So* CcP can accommodate electron donor binding in several possible orientations and that the presence of the MBP tag affects the availability of certain binding sites. To further investigate the structural basis of reductive activation in *So* CcP, we introduced mutations into two different regions of the protein that have been suggested to be important for reductive activation in homologous bacterial CcPs. Mutations in a flexible loop region neighboring the low-potential heme significantly increased the activation rate, confirming the importance of flexible loop regions of the protein in converting the inactive, as-isolated enzyme into the activated form.

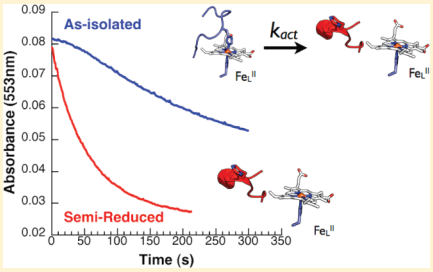

Reactive oxygen species such as hydrogen peroxide and superoxide are generated under hypoxic conditions as a result of a leaky or inefficient electron transport chain,[1] which may further yield toxic hydroxyl radicals through Fenton chemistry.[2] For many Gram-negative bacteria, it is thought that periplasmic peroxide scavenging is achieved by soluble diheme cytochrome *c* peroxidases.[3] Bacterial diheme cytochrome *c* peroxidases (BCcPs) differ from the canonical monoheme peroxidases such as horseradish peroxidase (HRP)[4] and yeast cytochrome *c* peroxidase (*y*CcP)[5] in their cofactor content and mechanism. The two heme cofactors in bacterial peroxidase enzymes are covalently bound within two separate cytochrome *c*-like domains. In all characterized BCcPs, the high-potential (approximately 330 mV vs NHE) Met-His ligated heme ("H-heme") serves as an electron transfer site, while the other low-potential "L-heme" (approximately −300 mV vs NHE) serves as the peroxidatic active site.[6,7] In the as-isolated state of the BCcP, both heme sites are in the ferric oxidation state, with the H-heme in a low-spin−high-spin equilibrium and the L-heme in a low-spin state.[7] The high-potential heme, which is not present in monoheme peroxidases, may store a second oxidizing equivalent during the catalytic cycle[6] and is hypothesized to mediate the transfer of electrons from electron donor proteins to the peroxidatic heme.[8,9]

Most BCcPs are isolated in a state that is catalytically inactive where both hemes are each in the ferric state, as exemplified by the diheme peroxidase from *Pseudomonas aeruginosa* (*Psa*).[10] In the absence of reducing equivalents provided by an electron donor protein or small molecule such as ascorbate, both hemes of the BCcP remain in the ferric state where the active site is bis-His-ligated, preventing binding of the peroxide substrate,[11] as illustrated in Figure 1. The active form of the enzyme can be achieved by a one-electron reduction termed "reductive activation": reduction of the H-heme results in local conformational changes that cause reorientation of the liganding groups on the low-potential heme, allowing for peroxide to access the active site (Figure 1B[11−13]). The overall phenomenon of reductive activation may serve a regulatory role, preventing turnover of the peroxidase in the absence of sufficient reducing equivalents provided by periplasmic electron donor proteins.

The reductive activation process is an essential step in most of the known BCcPs. In addition to the *Psa* enzyme,[10] reductive activation is required for the BCcPs from *Paracoccus denitrificans* (*Pd*),[14] *Pseudomonas nautica* (*Psn*),[15] *Rhodobacter capsulatus* (*Rc*),[16] *Pseudomonas stutzeri* (*Pss*),[17] and *Geobacter sulfurreducens* (*Gs*).[18] In contrast, diheme peroxidases from *Nitrosomonas europaea* (*Ne*)[19] and *Methyloccocus casulatus* (Bath)[20] do not need to undergo the activation step; the crystal structure of *Ne* CcP shows that the low-potential heme is

Received: March 24, 2011
Revised: January 11, 2012
Published: January 12, 2012

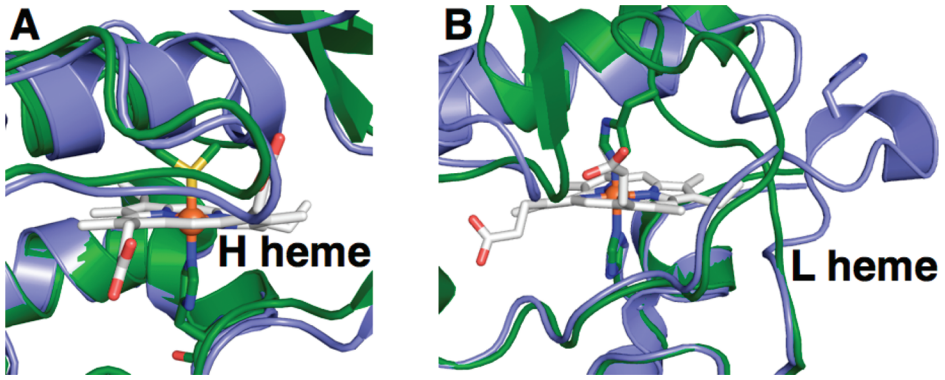

Figure 1. Comparison of the structures of the inactivated (green) and activated (blue) states of BC*c*Ps, focusing on the residues surrounding the high-potential heme (A) and low-potential heme (B). *P. aeruginosa* cytochrome *c* peroxidase as isolated is colored green [Protein Data Bank (PDB) entry 1EB7]; constitutively active cytochrome *c* peroxidase from *Nitrosomonas europaea* is colored blue (PDB entry 1IQC).

```
                          L-Heme                    Loop 1
Gs    59 LYFEPRLSASHLISCNTCHNVGLGGGDLQATSTGHGWQKGPRNAPTVLNSVFNTAQFWDG 118
Psa   60 LFFDPRLSRSHVLSCNTCHNVGTGGADNVPTSVGHGWQKGPRNSPTVFNAVFNAAQFWDG 119
So    46 LFFEPRLSKSGFISCNSCHNLSTGGVDALPTSIGHHWQEGPINSPTVLNADFMLAQFWDG 105
Ne    51 LFFDPRLSKSGFISCNSCHNLSMGGTDNITTSIGHKWQQGPINAPTVLNSSMNLAQFWDG 110
                                          *     *  *
               Loop 2
Gs   119 RAKDLAEQAKGPVQASVEMNNTPDQVVKTLNSIPDYVALFKKAFPGEKDPVTFDNMAKAI 178
Psa  120 RAKDLGEQAKGPIQNSVEMHSTPQLVEQTLGSIPEYVDAFRKAFPKAGKPVSFDNMALAI 179
So   106 RASNLKEQAAGPIANPKEMGFTHELATETIASMPAYRARFAKVYGDEK--VDIDRLTDAI 163
Ne   111 RAKDLKEQAAGPIANPKEMASTHEIAEKVVASMPQYRERFKKVFGSDE--VTIDRITTAI 168

                                                 H-Heme
Gs   179 EVFEATLITPDSPFDQYLKGKKKALDGKQTAGLKLFLDKGCVACHGGLNLGGTGYFPFGV 238
Psa  180 EAYEATLVTPDSPFDLYLKGDDKALDAQQKKGLKAFMDSGCSACHNGINLGGQAYFPFGL 239
So   164 AAFEKTLVTPNSPFDQYLLGKQDAISGDAKAGYQLFKDKGCVSCHNGPAVGGTMFMKMGL 223
Ne   169 AQFEETLVTPGSKFDKWLEGDKNALNQDELEGYNLFKGSGCVQCHNGPAVGGSSYQKMGV 228
                                                        *
                    Loop 3
Gs   239 VEKPAENILPLGDKGRFAVTNTAKDEYVFRAPSLRNVAITYPYFHSGVVWSLKEAVAVMG 298
Psa  240 VKKPDASVLPSGDKGRFAVTKTQSDEYVFRAAPLRNVALTAPYFHSGQVWELKDAVAIMG 299
So   224 IK-PFHTNNPAE--GRKGVTGKDADKFVFKVPTLRNIELTYPYFHDGSVWTLEEAVNTMA 280
Ne   229 FK-PYETKNPAA--GRMDVTGNEADRNVFKVPTLRNIELTYPYFHDGGAATLEQAVETMG 285
                                      *
```

Figure 2. Partial sequence alignment of various bacterial C*c*Ps: *Gs*, *G. sulfurreducens*; *Psa*, *P. aeruginosa*; *So*, *S. oneidensis*; *Ne*, *N. europaea*. Heme binding motifs (CXXCH) are highlighted in purple, and the three loop regions implicated in reductive activation are highlighted in yellow, blue, and orange.

pentacoordinate in the as-isolated form[13] (Figure 1B, blue). A sequence alignment of representative BC*c*P enzymes (Figure 2) shows that the sequences of key loop regions that undergo a change in conformation during reductive activation differ between *Psa*-type C*c*Ps that require reductive activation and *Ne* C*c*P, which does not. Swapping only two amino acids in one of these loop regions in the *Psa*-type C*c*P from *G. sulfurreducens* generates a constitutively active protein, mimicking the *Nitrosomonas*-like class of BC*c*Ps.[18] Intriguingly, on the basis of sequence, the *Shewanella oneidensis* (*So*) C*c*P is highly similar to *Ne* C*c*P (60% identical in terms of primary amino acid sequence) and diverges more strongly from *Psa*-like C*c*Ps (44% identical to *Psa* C*c*P). The sequence similarities between *Ne* and *So* are particularly striking in the flexible loop regions that have been identified as mediators of the conformational changes in reductive activation. We sought to test the hypothesis that, on the basis of sequence identity, the *So* C*c*P should be a member of the *Ne*-type functional subclass of BC*c*Ps, which would not require reductive activation.

In this report, we characterize the peroxidase activity of a diheme peroxidase from *S. oneidensis*.[42] We express the *So* C*c*P gene (SO2178) recombinantly in *Escherichia coli* as a maltose-binding protein fusion that has been previously described,[21] as well as the redox partner for *So* C*c*P, a monoheme cytochrome c_5, SO0264.[21,42] We show, on the basis of EPR, UV−visible spectroscopy, and steady-state kinetics of recombinant *So* C*c*P, that the *So* C*c*P is a conventional *Psa*-type BC*c*P requiring reductive activation. We find that the as-isolated form of *So* C*c*P undergoes rapid reductive activation under in vitro assay conditions, with a rate that depends on the concentration of the electron donor. We present a computational model for the peroxidase activity of as-isolated *So* C*c*P that permits the deconvolution of the reductive activation rate and the peroxide turnover rate from the enzymatic progress curves. Following our initial characterization of the *So* C*c*P system, we demonstrate that this protein serves as a facile model system for structure−function analysis through further investigation of the role of the activation loops of *So* C*c*P. We show that mutations in loop 1 and loop 3 regions do not completely inhibit peroxidase activity but instead

dx.doi.org/10.1021/bi201135s | *Biochemistry* 2012, 51, 974−985

reveal defects in peroxidase turnover and increases in the activation rate.

MATERIALS AND METHODS

Expression and Purification of Diheme Cytochrome *c* Peroxidase from *S. oneidensis*. The gene encoding the *Shewanella* cytochrome *c* peroxidase (SO2178) in parent vector pMKL1 was a kind gift to our laboratory from F. Collart and Y. Londer (Argonne National Laboratory, Argonne, IL). The SO2178 gene was expressed as a fusion to the C-terminus of the maltose-binding protein (MBP), with a TEV site between the MBP and *So* C*c*P to allow isolation of a tag-free *So* C*c*P protein. The MBP protein also included an N-terminal hexahistidine tag for Ni^{2+} affinity purification. The *So* C*c*P–MBP fusion protein was expressed in *E. coli* JM109 cells (Strategene). Maximal *So* C*c*P expression was achieved by cotransformation with pEC86, a plasmid bearing the cytochrome *c* maturation cassette.[22] Transformed cells were grown in a 10 mL starter culture at 37 °C for 8 h. Starter cultures were resuspended in fresh medium and used to inoculate bulk expression cultures containing 1 L of 2× YT (Fisher BioReagents) supplemented with 100 μg/mL ampicillin and 25 μg/mL chloramphenicol in a 2 L flask. Bulk expressions were grown at 37 °C for 14–16 h with good aeration (200 rpm) to high optical density (A_{600} > 2). Induction for 4 h with 80 mg/L IPTG yielded pink to brown pellets as an indication of cytochrome *c* production. Cells were harvested, sonicated in 20 mM Tris (pH 7.4), 150 mM NaCl, 100 μM EDTA, and 0.13 mg/mL lysozyme, clarified by centrifugation, and immediately loaded onto an amylose affinity resin column (NEB) to avoid proteolytic cleavage of the C*c*P–MBP fusion protein. For sensitive applications requiring very pure samples, amylose chromatography was followed by size exclusion chromatography on an S-100 column (GE Healthcare prepacked HiPrep Sephacryl). Removal of MBP was achieved by cleavage overnight with TEV protease and subsequent Ni^{2+}-NTA chromatography. *So* C*c*P mutants in loop 1 (P75T/H81K/E84Q) and loop 3 (M219Q/F247N) were constructed using the QuikChange Mutagenesis Kit [Stratagene (see the Supporting Information)] and expressed and purified as MBP fusions as described for the wild-type protein.

Expression and Purification of Recombinant *P. aeruginosa* Azurin. Plasmid pETAz9[+] was a kind gift of M. McGuirl (University of Montana, Missoula, MT). The plasmid was transformed into *E. coli* BL21(DE3), and the transformants were grown in 4 mL starter cultures of 2× YT until they became cloudy. Starter cultures were used to inoculate 1 L cultures of 2× YT with 50 μg/mL kanamycin for bulk expression. The 1 L cultures were grown at 37 °C overnight, reaching a high optical density, and induced in the morning with 1 mM IPTG for 4 h. The resulting cells were lysed gently by sonication in buffer containing 20 mM Tris (pH 8), 20% glucose, 15 μg/mL lysozyme, and 5 μg/mL DNase. The clarified lysate was supplemented with a final $CuSO_4$ concentration of 100 μM, and holo-azurin was loaded on Q-Sepharose equilibrated in 10 mM diethanolamine (pH 9). Azurin was eluted with 500 mM NaCl in 10 mM diethanolamine (pH 9.00). Azurin-containing fractions were reduced with 1 mM dithionite and further purified by size exclusion chromatography (GE Healthcare prepacked HiPrep Sephacryl S-100).

Expression and Purification of *S. oneidensis* Cytochrome c_5. *S. oneidensis* gene SO0264, which encodes cytochrome c_5, was synthesized by Genewiz and subcloned into pET25b+ (Invitrogen) at the EcoRV restriction site. The resulting plasmid was named pSOc5 and was used for the expression of a tag-free version of the cytochrome bearing the wild-type periplasmic localization sequence at the N-terminus. Recombinant *S. oneidensis* cytochrome c_5 was expressed in *E. coli* BL21(DE3) carrying the pEC86 plasmid.[22] For overexpression, 1 L of 2× YT medium containing 100 μg/mL ampicillin and 25 μg/mL chloramphenicol was inoculated with 5 mL of resuspended overnight BL21(DE3)/pEC86/pSOc5 culture and grown without IPTG induction at 37 °C for 22 h with moderate shaking (170 rpm). Cell pellets were harvested by centrifugation, resuspended in 80 mL of lysis buffer [20 mM Tris (pH 8), 1 mM EDTA, 50 mM NaCl, and 0.1 mg/mL lysozyme], and lysed by sonication. Lysate was clarified by centrifugation; the pH of the clarified lysate was adjusted to 4.5 by dropwise addition of 1 M acetic acid, and precipitated proteins were removed by centrifugation. The resulting pink supernatant was oxidized by addition of an equimolar amount of potassium ferricyanide and loaded onto MacroPrep HighS resin [10 mL bed volume (Bio-Rad)] equilibrated in 10 mM sodium acetate (pH 4.5). Bound proteins were eluted with an 80 mL gradient from 50 to 500 mM NaCl in 10 mM sodium acetate (pH 4.5). *So* cytochrome c_5 eluted in a broad peak centered around 250 mM NaCl, and fractions with purity ratios (A_{410}/A_{280}) of ≥4.0 were pooled and stored in 15% glycerol at −80 °C.

EPR Spectroscopy. X-Band (9.62 GHz) EPR spectra were recorded on a Bruker 300 spectrometer equipped with an Oxford ESR-910 liquid helium cryostat. The quantification of all signals is relative to a Cu-EDTA spin standard. For quantification, the spectra were recorded under nonsaturating microwave conditions, meaning that the signal intensity was found to be proportional to the square root of the microwave power. The EPR spectrum of the Cu-EDTA standard was recorded daily at a temperature of 10 K and a microwave power of 2 μW. The copper concentration of the standard was determined by atomic absorption. The microwave frequency was calibrated with a frequency counter and the magnetic field with a nuclear magnetic resonance (NMR) gaussmeter. The sample temperature was calibrated with a carbon-glass resistor (LakeShore CGR-1-1000) placed at the position of the sample in an NMR tube. A modulation frequency of 100 kHz with a 10 G modulation amplitude was used for all EPR experiments. The EPR simulation software was written by one of the authors. The simulations are least-squares fits of the experimental spectra generated with consideration of all intensity factors, which allows computation of simulated spectra for a specified sample concentration. The simulations therefore allow a quantitative determination of protein signal intensities. The Windows software package (SpinCount) is available for general application to any mono- or dinuclear metal complex by contacting M. P. Hendrich.

Activity Assays. The properties of the electronic absorption spectra of the C*c*P–MBP fusion protein and the tag-free C*c*P were determined on a Cary 50 spectrophotometer (Varian). All assays were conducted at 23 °C in assay buffer [5 mM MES, 5 mM HEPES, 10 mM NaCl, and 1 mM $CaCl_2$ (pH 6.00)] following the protocol previously reported for the *Pd* enzyme.[14] Horse heart cytochrome *c* (Sigma), *Psa* azurin, or *So* cytochrome c_5 was reduced by treatment with 20 mM sodium L-ascorbate, and excess ascorbate was removed from the electron donor with a PD-10 desalting column (NEB) immediately before the assay. A stock of 5–10 μM enzyme was prepared in assay buffer. As-isolated proteins were treated with $K_3Fe(CN)_6$ to ensure that the enzyme was fully oxidized. The semireduced enzyme was prepared by incubation for at least 1 h in 1 mM sodium L-ascorbate and 10 μM diaminodurol. The oxidation of the reduced horse heart cytochrome *c* was monitored at 550 nm

in the presence of H_2O_2 using an extinction coefficient difference between the oxidized and reduced protein ($\Delta\varepsilon_{550}$) of 21.5 mM^{-1} cm^{-1},[23] whereas oxidation of reduced *So* cytochrome c_5 was monitored at 553 nm using a difference in extinction coefficients ($\Delta\varepsilon_{553}$) of 12.5 ± 2 mM^{-1} cm^{-1} as determined by comparison to protein concentrations determined by the BCA assay (Thermo Scientific). When azurin was used as the electron donor, the increase in absorbance at 628 nm was monitored using an extinction coefficient (ε_{628}) of 5.0 mM^{-1} cm^{-1}.[24]

Lag-Phase Kinetic Model. A kinetic model for activation of the fully oxidized enzyme was implemented in Python 2.7, and the complete code is given in the Supporting Information. Because the concentration of the active, semireduced C*c*P enzyme changes over the course of the experiment, the differential equations that describe the behavior of the system do not have a closed solution. Instead, we implement numerical integration with a time step of 0.2 s to find an approximate analytical solution to the differential equations. Least-squares optimization was accomplished using the optimize.leastsq function in SciPy.

The amount of C*c*P converted from the as-isolated, oxidized state to the semireduced state during each time step depends on both the fraction of oxidized C*c*P that is bound to an electron donor and the rate of electron transfer in the bound complex. On the basis of the observation that even high concentrations of electron donor proteins (>50 μM) are not saturating in the peroxidase assay, we assume that binding of oxidized C*c*P to the reduced electron donor (ED) protein has an equilibrium dissociation constant of >10 μM and can be modeled by a rapid equilibrium. The fraction of oxidized C*c*P in the bound complex is given by

$$f_B = \frac{[ED]_{red}}{[ED]_{red} + K_D}$$

where $[ED]_{red}$ is the concentration of the reduced electron donor and K_D is the equilibrium dissociation constant for the reduced electron donor binding to oxidized C*c*P.

During each time step, the concentration of semireduced C*c*P increases by the factor

$$\Delta[CcP]_{active} = k_{act} f_B [CcP]_{inactive}$$

where k_{act} is a rate constant with units of s^{-1} that describes the rate of electron transfer in the bound complex.

During each time step, there are two ways for the electron donor to become oxidized. The first is donating an electron to activate one molecule of C*c*P. The second is donating an electron to a molecule of C*c*P that has been oxidized by peroxide during the catalytic cycle. C*c*P must be recharged with two electrons during each catalytic cycle.[6] The rate of peroxide catalysis depends on $[CcP]_{active}$ and is first-order in terms of the reduced electron donor concentration. To ensure the reaction is zeroth-order in peroxide, we use peroxide concentrations in excess of 9 μM, a value 1 order of magnitude greater than the hydrogen peroxide K_m (see Results). The total change in the concentration of the reduced electron donor at each time step is

$$\Delta[ED]_{red} = \Delta[CcP]_{active} + 2k_1[CcP]_{active}[ED]_{red}$$

where k_1 is the second-order rate constant for peroxide turnover. Multiplying k_1 by the electron donor concentration gives a first-order rate constant that should match the k_{cat}^{obs} from Michaelis–Menten analysis.

The total absorbance was calculated using extinction coefficients for oxidized and reduced forms of the electron donor. For horse heart cytochrome *c*, ε(550 nm, oxidized) = 8.4 mM^{-1} cm^{-1} and ε(553 nm, reduced) = 29.9 mM^{-1} cm^{-1}.[23] For *S. oneidensis* cytochrome c_5, extinction coefficients were experimentally determined by comparison to BCA assay-derived concentrations: ε(553 nm, oxidized) = 5.1 ± 0.5 mM^{-1} cm^{-1}, and ε(553 nm, reduced) = 17.6 ± 2 mM^{-1} cm^{-1}.

Following these three calculations, new values for $[CcP]_{active}$, $[CcP]_{inactive}$, $[ED]_{ox}$, and $[ED]_{red}$ were calculated and used as initial values for the next time step. For the best fit to the data, we included an additional time-dependent decay of the active *So* C*c*P into an inactive state.

RESULTS

Expression and Purification of *So* C*c*P as an MBP Fusion Protein. The bacterial diheme peroxidase from *S. oneidensis* was overexpressed in *E. coli* JM109 as a soluble MBP fusion protein. Induction at a high optical density (A_{600} > 1) in the presence of the *c*-type cytochrome maturation cassette (*ccm*ABCDEFGH)[22] yields 10–25 mg of fusion protein per liter of culture. Because the presence of a fusion protein can change the activity of the protein of interest,[25,26] we proceeded to investigate whether the recombinant protein behaved like a native BC*c*P in biochemical assays.

Following removal of the MBP protein by TEV protease and Ni-NTA chromatography, the purity index (A_{408}/A_{280}) was typically around 4.8, matching previously reported values for bacterial diheme peroxidases isolated from their native sources.[27] Because all bacterial diheme peroxidases have two hemes and a comparable number of tryptophan residues, a similar purity index suggests that a majority of the protein has native heme loading. The MBP fusion protein runs on an sodium dodecyl sulfate–polyacrylamide gel electrophoresis (SDS–PAGE) gel with an apparent molecular mass of 70 kDa, and the tag-free *So* C*c*P runs in a diffuse band with an apparent molecular mass of 35 kDa (Figure S1 of the Supporting Information), consistent with the size predicted by the expressed amino acid sequence. Like all other reported BC*c*Ps, both the MBP fusion and tag-free *So* C*c*P proteins run as a dimer via size-exclusion chromatography (Figure S2 of the Supporting Information).[16,19,20,28]

Optical Properties of the C*c*P–MBP Fusion Protein and Tag-Free C*c*P. The optical absorbance spectra of fully oxidized versus semireduced *So* C*c*P, both as an MBP fusion protein and with the MBP tag removed, are shown in Figure 3. The spectral features at wavelengths greater than 300 nm characteristic of heme absorption are virtually identical in the *So* C*c*P–MBP fusion protein and the tag-free *So* C*c*P, suggesting that the heme environments are not substantially affected by the presence of the fusion protein. The fusion protein has a higher absorbance at 280 nm, consistent with the presence of additional tryptophans in the MBP tag. Semireduced samples have extremely high absorbance at wavelengths below 300 nm because of the presence of excess sodium L-ascorbate, which is required to keep the sample in the semireduced state.

Fully oxidized *So* C*c*P shows a characteristic Soret maximum at 407 nm and broad β- and α-bands at 540 and 553 nm, respectively. The fully oxidized enzyme does not display the 640 nm band indicative of high-spin heme (Figure 3, inset). Upon reduction with L-ascorbate, the Soret band maximum shifts to 417 nm and a Soret shoulder around 407 nm persists, the β- and α-bands at 540 and 553 nm, respectively, become dramatically sharper (consistent with the reduction of the

dx.doi.org/10.1021/bi201135s | *Biochemistry* 2012, 51, 974–985

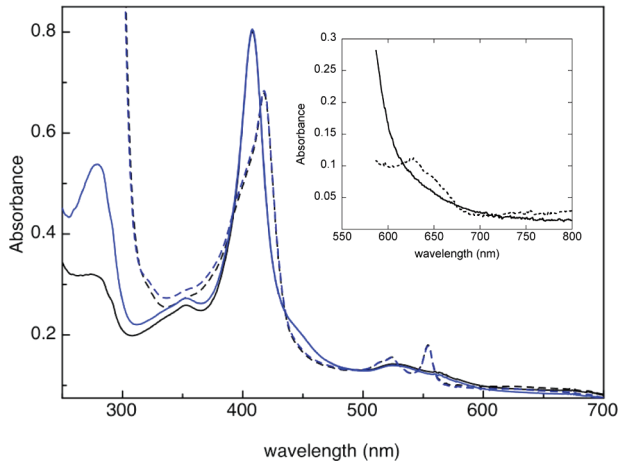

Figure 3. Electronic absorption spectra of the oxidized (solid black line) and semireduced (dashed black line) tag-free *So* C*c*P and oxidized (solid blue line) and semireduced (dashed blue line) *So* C*c*P–MBP fusion. The inset shows the absorption spectra of tag-free oxidized and semireduced *So* C*c*P at an 8-fold higher concentration.

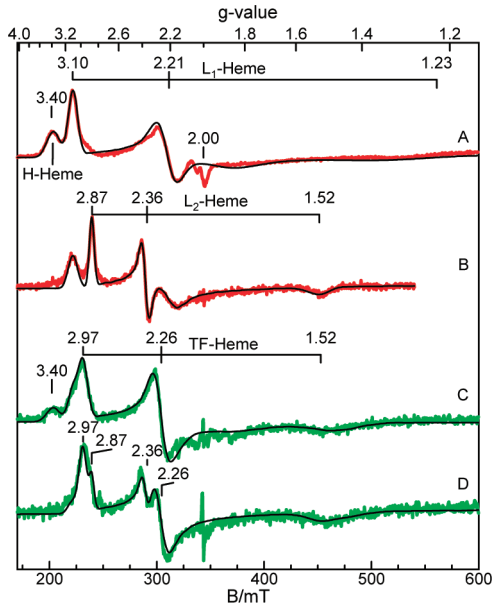

Figure 4. EPR spectra of 0.5 mM C*c*P in the absence and presence of sodium L-ascorbate with simulations overlaid: (A) *So* C*c*P–MBP fusion, (B) semireduced *So* C*c*P–MBP fusion, (C) tag-free *So* C*c*P, and (D) semireduced tag-free *So* C*c*P. Experiments were conducted at a microwave frequency of 9.62 GHz, a power of 0.02 mW, and a temperature of 7 K.

H-heme[29]), and a charge transfer band at ~640 nm, suggestive of a high-spin ferric heme state, is clearly apparent (Figure 3, inset).

EPR Properties of the C*c*P–MBP Fusion Protein and Tag-Free C*c*P. The fully oxidized state of *So* C*c*P shows two low-spin ferric species (Figure 4A) in equal amounts. The g = 3.40 signal is from a highly anisotropic low-spin species observed in all bacterial diheme peroxidases in their as-isolated state (both hemes in the ferric state) and originates from the H-heme of the protein.[17,19,30,31] Species with g = 3.0, 2.21, and 1.30 signals (L_1-heme) originate from the L-heme and have g values similar to that of the *Psa*-type peroxidases.[31,32] The simulation overlaid on the data quantitatively agrees with the total heme concentration of the sample, and from the simulation, the two heme species are found to be present in equal amounts. *So* C*c*P does not show a high-spin ferric signal near g = 6, which is a minority species in other diheme peroxidases (Figure S3 of the Supporting Information).[17,19,29,30,33] Upon reduction with ascorbate, the H-heme signal disappears (Figure 4B), suggesting conversion of the ferric H-heme to an EPR silent low-spin ferrous species as observed in other peroxidases. The signal from the L_1-heme loses intensity, and a new low-spin heme species with g = 2.87, 2.36, and 1.51 signals (L_2-heme) appears. This change can be attributed to the conversion of a fraction of the low-potential species into the new L_2-heme species. The concentrations of L_1- and L_2-heme in the semireduced C*c*P together account for the concentration of low-potential heme before reduction. Table 1 summarizes the various species in the oxidized and semireduced enzyme with their amounts obtained from quantitative simulations.

Tag-free *So* C*c*P (Figure 4C) shows the same H-heme species and L_1-heme species as the fusion protein, but both in overall smaller amounts (Table 1). In addition, a new feature is observed at g = 2.97. The new signal represents a significant amount of heme and overlaps with the g = 3.10 signal of the L_1-heme. As shown by the simulation in Figure 4C, the spectrum can be accurately simulated with three heme species, using the same parameters as for H- and L_1-heme species, and a new heme site with g = 2.97, 2.26, and 1.52 signals (TF-heme). The simulations indicate that the concentrations of the H- and L_1-heme species are approximately equal, and the amounts of both are smaller, commensurate with the amount of TF-heme present. Thus, the new TF-heme species appears at the expense of both H- and L_1-heme species. For the semireduced tag-free protein (Figure 4D), the g = 3.40 signal vanishes, indicating full reduction of the H-heme. The magnitude of the g = 3.1 signal (shoulder) decreases, and the signal from the L_2-heme is clearly visible at g = 2.36. The simulation shown in Figure 4D uses the same parameters for L_1-, L_2-, and TF-hemes that were used in Figure 4B or 4C, except in different amounts. The percentages of species determined from the simulation are listed in Table 1. The relative amounts of the L_1- and L_2-heme species are consistent with that observed from the fusion protein. The TF-heme species in the semireduced sample is not affected by ascorbate addition, and the amount of this species remains the same before and after reduction.

Table 1. EPR Parameters of the C*c*P–MBP Fusion Protein and Tag-Free *So* C*c*P in the Oxidized and Semireduced States

	amount with respect to total Fe (%)			
heme	C*c*P–MBP fusion	semireduced C*c*P–MBP fusion	tag-free C*c*P	semireduced tag-free C*c*P
H-heme	50	0	33	0
L_1-heme	50	34	33	11
L_2-heme	0	20	0	8
TF-heme	0	0	33	33

Catalytic Properties of *So* C*c*P. The activity of *So* C*c*P was determined in the presence of micromolar concentrations of various redox partners (Table 2). *So* cytochrome c_5 is the native electron donor in the periplasm of *Shewanella*,[42] whereas horse heart cytochrome *c* and azurin are electron donors that have been previously used for kinetic analysis of BC*c*Ps and are

dx.doi.org/10.1021/bi201135s | *Biochemistry* 2012, 51, 974–985

Table 2. Kinetic Parameters of the Oxidized and Semireduced States of the *So* CcP−MBP Fusion Protein and Tag-Free *So* CcP

		CcP−MBP fusion		tag-free CcP	
electron donor[a]	parameter[b]	semireduced	oxidized	semireduced	oxidized
horse heart cytochrome *c*	K_m (μM) for H_2O_2	0.13 ± 0.08	0.3 ± 0.1	0.03 ± 0.01	0.17 ± 0.05
	k_{cat}^{obs} (s^{-1})	35 ± 3	13 ± 1	1.9 ± 0.2	1.3 ± 1.0
	k_{cat}^{obs}/K_m ($\times 10^6$ M^{-1} s^{-1})	280	46	74	7.5
So cytochrome c_5	K_m (μM) for H_2O_2	0.1 ± 0.1	0.8 ± 0.1	0.3 ± 0.1	0.6 ± 0.5
	k_{cat}^{obs} (s^{-1})	10 ± 1	0.8 ± 0.1	73 ± 5	7 ± 5
	k_{cat}^{obs}/K_m ($\times 10^6$ $M^{-1}s^{-1}$)	100	1	240	12
azurin	K_m (μM) for H_2O_2	0.2 ± 0.2	0.3 ± 0.1	0.2 ± 0.1	0.4 ± 0.1
	k_{cat}^{obs} (s^{-1})	40 ± 20	12 ± 2	3.4 ± 0.3	1.3 ± 0.1
	k_{cat}^{obs}/K_m ($\times 10^6$ $M^{-1}s^{-1}$)	202	38	17	3

[a]Electron donors are horse heart cytochrome *c* (10 μM), *So* cytochrome c_5 (4 μM), and azurin (12 μM). [b]Assays were conducted in 5 mM MES, 5 mM HEPES, 10 mM NaCl, and 1 mM $CaCl_2$ (pH 6.0) at 23 °C.

included in this study for comparison. We determined kinetic parameters for both the *So* CcP−MBP fusion and tag-free *So* CcP. The linear initial rates (for the semireduced protein) or fastest linear phases (for the oxidized protein) at various concentrations of peroxide were used to calculate kinetic parameters using the Michaelis−Menten formalism (Table 2 and Figure S4 of the Supporting Information). Because the electron donor proteins bind extremely weakly to *So* CcP (K_m > 10 μM), we could not achieve saturating concentrations in vitro using any of the electron donors studied, and as a result, the values reported here are not maximal turnover rates.

Qualitative inspection of the progress curves reveals that while the oxidation of the electron donor occurs in a typical manner for reactions initiated by the semireduced enzyme (Figure 5A), a distinct lag phase is observed when fully oxidized *So* CcP is used (Figure 5B). The lag phase reflects the conversion of the oxidized state to the active, semireduced state in vitro. In all cases, k_{cat}^{obs} values for the semireduced *So* CcP are greater than those of oxidized *So* CcP. We suspect that this is partially because of a time-dependent deactivation of the CcP during the several-minute time course of the experiment. We have seen that for both semireduced and oxidized *So* CcP, the electron donor is not completely oxidized at the end point of the experiment if the initial rate is not sufficiently fast (data not shown).

Kinetic parameters for *So* CcP vary depending on the electron donor used or the presence of the MBP tag. For the non-native electron donors horse heart cytochrome *c* and azurin, peroxide turnover of the MBP-tagged *So* CcP is approximately 10 times faster than for the native, tag-free form in the same oxidation state. In contrast, when *So* cytochrome c_5 is used, the opposite is true; peroxide turnover rates for the tag-free protein are 7−10 times faster for the tag-free form of the protein than for the MBP-tagged protein, suggesting that the MBP tag affects the rate-limiting step of turnover.

Peroxide binding as assessed by K_m values is the same, within error, for almost all combinations of peroxidases and electron donors assayed. A notable exception is that K_m values are generally 2 times weaker for the oxidized form of the enzyme than for the semireduced form under the same conditions, which may reflect an incomplete activation of the oxidized protein on the time scale of the in vitro assay.

Comparison of Peroxide Turnover Parameters to Those of Other BCcP Family Members. Peroxide turnover kinetics have been reported for numerous members of the BCcP family (Table 3). Among the BCcPs in Table 3, all have estimated or measured K_m values for electron donors of >50 μM.[17,20,24,34] Because peroxide turnover was assessed at concentrations much lower than the K_m, the rate of the reaction is approximately linearly proportional to the electron donor concentration. In this linear range, the peroxide turnover divided by the electron donor concentration (k_{cat}^{obs}/[ED]) gives an effective bimolecular rate constant that can be compared between the BCcPs. The value of k_{cat}^{obs}/[ED] for *So* CcP is the fastest of the values of all of the BCcPs we surveyed. *So* CcP also has the tightest peroxide binding, as measured by K_m.

Computational Modeling of Lag-Phase Kinetics. Our simple kinetic model, which considers an equilibrium binding step, an activation step, and a peroxidase turnover step, recapitulates the shape of the peroxide turnover progress curve (Figure 5C). Residuals are very small but nonrandom, suggesting a minor systematic error of unknown origin.

Implementing the computational model requires us to make some educated hypotheses about the *So* CcP−*So* cytochrome c_5 system. The model contains two different parameters, the activation rate and the dissociation constant for binding of the electron donor to *So* CcP, either of which could effect the length of the lag phase. Neither of these parameters has been measured independently for *So* CcP or *So* cytochrome c_5. In our model, we are unable to separate the effect of the activation rate constant from that of the equilibrium dissociation constant of the oxidized form of *So* CcP for the reduced electron donor. We therefore implement the model by keeping the equilibrium dissociation constant the same (7 μM) for all cases. This value for K_D is in the range of equilibrium binding constants previously reported for BCcPs and monoheme electron donor proteins.[9] Differences in the activation rates that we report (k_{act}) reflect either changes in the electron transfer rate or differences in binding of the electron donor.

Analysis of lag-phase kinetics using the computational model (Table 4) confirms the results from Michealis−Menten analysis. The *So* CcP−MBP fusion turns over peroxide at approximately the same rate with either horse heart cytochrome *c* or *So* cytochrome c_5 as the electron donor, whereas tag-free *So* CcP turns over peroxide 25 times more rapidly with the native electron donor *So* cytochrome c_5 than with horse heart cytochrome *c*. Activation rates are significantly slowed when tag-free *So* CcP is assayed in the presence of horse heart cytochrome *c* as the electron donor. This suggests that horse heart cytochrome *c* binds to the tag-free protein either more weakly or in a conformation that gives less efficient electron transfer.

Characterization of Activation Loop Mutants. Additional kinetic analyses were performed for two tag-free *So* CcP variants containing mutations in two of the three loops that are known to undergo conformational changes upon reductive

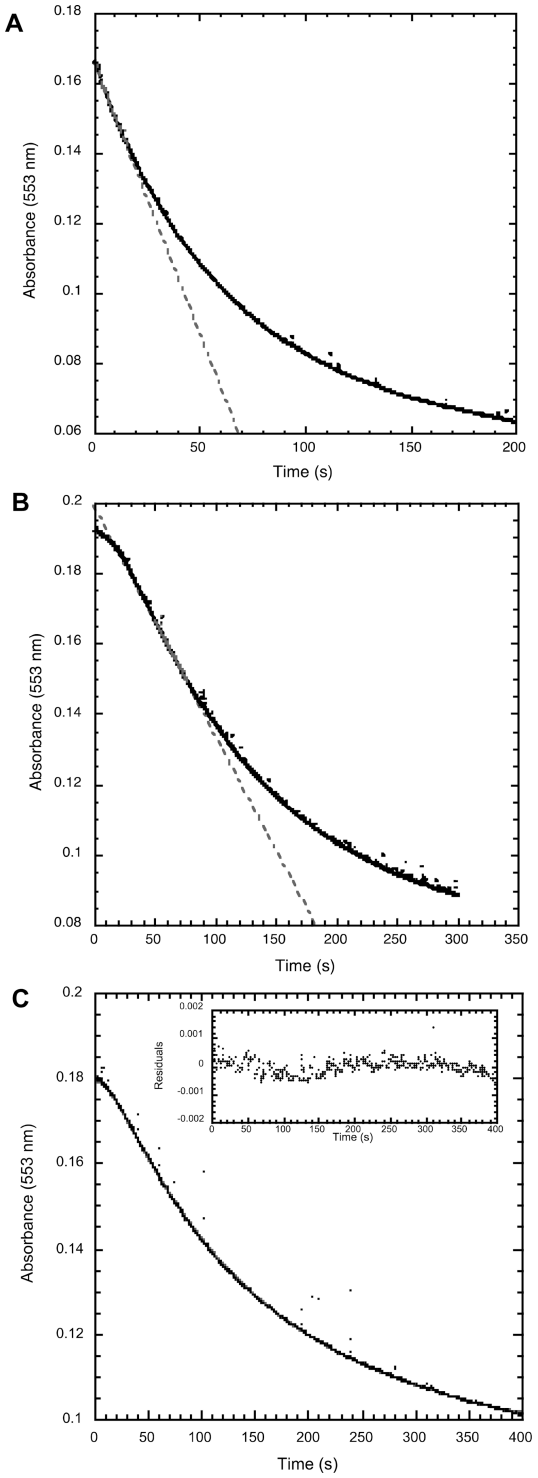

Figure 5. Comparison of peroxidase catalytic activity using *So* cytochrome c_5 (4 μM) as the electron donor for (A) semireduced tag-free *So* C*c*P and (B and C) oxidized tag-free *So* C*c*P. Experiments were conducted in 5 mM MES, 5 mM HEPES, 10 mM NaCl, and 1 mM $CaCl_2$ (pH 6.0) at 23 °C. In panels A and B, points represent the data and a line represents the linear rate used for Michaelis–Menten analysis. Panel C compares the experimental data (points) to the least-squares fit of the data to the kinetic model (line) as described in the text. The inset in panel C shows the residuals of the least-squares fit.

activation of a *Psa*-type C*c*P (depicted in Figure 1): either loop 1 (P75T/H81K/E84Q) or loop 3 (M219Q/F247N). We did not introduce mutations into the loop 2 region because the amino acid sequence of the *So* enzyme already matches that of the *Ne* C*c*P in all key positions that are different between the two functional subclasses. The visible absorbance spectra of both *So* C*c*P variants in the semireduced and oxidized states are identical to the spectrum of the wild-type protein in the same oxidation state (data not shown), indicating that the protein variants are folded with hemes in an environment similar to the wild-type enzyme. Despite the location of the mutations (many of which are far from the presumed peroxide binding site), both variants show defects in peroxide turnover (Table 5), suggesting that the wild-type enzyme is highly optimized for a high rate of peroxide turnover. The triple mutant in loop 1, P75T/H81K/E84Q, shows a 5-fold decrease in the rate of turnover of the semireduced state and a 20-fold decrease in the rate of turnover of the oxidized state compared to the wild-type protein under identical conditions. The double mutant, M219Q/F247N, shows a slightly larger defect in peroxide turnover in the semireduced state, a 12-fold decrease when compared to that of the wild-type protein under identical conditions. Peroxide binding for the semireduced state of the mutants, as measured by K_m, is unchanged (within error) for the mutants compared to that of the wild type, but both mutants show a slight increase in the K_m of the oxidized state for peroxide. The *So* C*c*P protein variants also demonstrated lag-phase kinetics for peroxide turnover when reactions were initiated by the oxidized enzyme. For the loop 1 triple mutant, the activation rate is 7 times faster than the wild-type rate, and the loop 3 double mutant shows a very slight increase in activation rate versus that of the wild type.

The kinetic differences noted for these two constructs were reflected in differences in their EPR characterization; whereas the fully oxidized wild-type MBP-tagged enzyme reveals two states H (g = 3.37, 2.20, and 1.50) and L_1 (g = 3.08, 2.26, and 1.30) corresponding to the H- and L-hemes, respectively, both the loop 1 triple mutant and the loop 3 double mutant additionally reveal significant population of states L_2 and TF (Figure S5 of the Supporting Information). Thus, substantial amounts (Table S1 of the Supporting Information) of oxidized MBP enzymes have already adopted conformations that would be associated with activated L-heme (i.e., the L_2 state). Consequently, the presence of lag-phase kinetics is at present unclear. The lower activities of the variants do not quantitatively correlate with the presence of the TF-heme. If we assume that the TF-heme state is inactive, we would expect a decrease in activity of at most a factor of 2, yet activity is decreased by approximately 1 order of magnitude. We suspect, but cannot yet substantiate, that the conformational changes observed in the EPR spectra of the oxidized states of the variants reflect changes in access to the hemes, their redox properties, or the ability of specific enzymatic states to interconvert, as required for catalysis.

DISCUSSION

Optical Spectroscopy of *So* C*c*P. The electronic absorption spectra of the as-isolated state of the MBP fusion protein and tag-free *So* C*c*P both exhibit the Soret maximum at 407 nm characteristic of ferric *c*-type hemes. Changes to the spectrum upon reduction with ascorbate or dithionite mirror changes that have been seen for other BC*c*Ps.[15,16,18,19,29] Reduction of the H-heme with ascorbate causes a red shift in the Soret maximum to 417 nm and a sharpening of the β- and α-bands at 540 and 553 nm, respectively, while the ascorbate-reduced spectrum maintains a Soret feature at 407 nm, indicating that one heme remains in the ferric state. Further reduction with dithionite results in the disappearance of the Soret

Table 3. Comparison of Literature Values of the Peroxide Turnover Parameters of Various Bacterial Diheme Cytochrome *c* Peroxidases in the Semireduced State Using Cytochrome *c* as an Electron Donor

organism[a]	K_m (μM) for H_2O_2	k_{cat}^{obs} (s^{-1})	electron donor (concentration)	k_{cat}^{obs}/[ED] (s^{-1} μM^{-1})[c]	required prereduction?	ref
Psa	6	118	*Psa* cytochrome c_{551} (13 μM)	14	yes	24
Rc[b]	33	40	*Rc* cytochrome c_2 (18 μM)	2	yes	34
Pss	1.8	88	*Pss* cytochrome c_{551} (7 μM)	13	yes	17
Gs	6.2	15.5	ABTS (3 mM)		yes	18
Mc	0.5	50	*Mc* cytochrome c_{555} (9 μM)	5	no	20
So	0.3	73	*So* cytochrome c_5 (4 μM)	18	yes	this study

[a]Abbreviations match those used in the text. [b]Turnover for the as-isolated protein. [c]This approximation holds because the concentration of the electron donor is much lower than the estimated K_m; therefore, the rate is approximately linear with electron donor concentration.

Table 4. Model-Derived Kinetic Parameters for Peroxidase Turnover Initiated with Oxidized Tag-free *So* CcP

electron donor	peroxidase	activation rate k_{act} (s^{-1})	peroxide turnover rate k_1 (s^{-1})[a]
So cytochrome c_5	*So* CcP–MBP	0.05 ± 0.01	1.6 ± 0.4
	So CcP	0.07 ± 0.02	7 ± 1
horse heart cytochrome *c*	*So* CcP–MBP	0.08 ± 0.02	1.6 ± 0.4
	So CcP	0.02 ± 0.007	0.28 ± 0.08

[a]Turnover values correspond to 4 μM electron donor, with the K_D for binding of the electron donor to CcP set to 7 μM.

shoulder and an increase in the intensity of the Soret peak at 417 nm (data not shown). Intriguingly, the only significant difference in the optical characteristics of the *So* enzyme, with respect to canonical CcPs, is the absence of a 640 nm band with the fully oxidized enzyme. As observed in the *Pd* and *Psa* enzymes, the 640 nm band has been attributed to a high-spin state of the high-potential heme.[29,30,33] Thus, the *So* enzyme appears to possess a low-spin H-heme. However, the 640 nm band is observed in the semireduced protein, indicating the same high-spin state of the oxidized L-heme, in parallel with other BCcP enzymes that require reductive activation to attain activity.[29,30,33]

EPR Characterization of *So* CcP. Comparisons of the *So* enzyme with other bacterial diheme peroxidases by electron paramagnetic resonance spectroscopy (EPR) demonstrate the similarity of *So* peroxidase to the *Psa*[30] and *Pd*[31] peroxidases in its oxidized and semireduced forms, as compared to the *Ne* and *Mc* peroxidases. In the oxidized state, the g_z value (3.10) of the L-heme is closer to that of *Pd* (3.00) than that of *Ne* (2.85). In the semireduced state of the *So* and *Pd* enzymes, a fraction of the L-heme changes to a new species, whereas no such change occurs for the *Ne* enzyme. In contrast to the results of optical spectroscopy, we observe no evidence in the EPR of conversion of heme to the high-spin state as has been previously observed for the *Psa* enzyme.[30] For the *So* enzyme, the two L-Heme species represent 34 and 20% of the heme in the sample after the addition of ascorbate. On the basis of the *g* values, the new L_2-heme species falls into the imidazolate classification of EPR signals: using the crystal field parameters of Taylor,[35] Δ/λ = 2.736 and v/Δ = 0.762 for L_2, while L_1 displays analogous parameters that are indicative of neutral imidazole binding (Δ/λ = 2.687, and v/Δ = 0.524). Thus, it appears that upon semireduction the axial His for 40% of the L-heme is deprotonated. For all these enzymes, the g_z values of the H-heme are approximately the same, and this heme is reduced with ascorbate in the semireduced form. Approximately one-half of the tag-free *So* CcP protein appears to be the same as the fusion protein. The signals are in the same locations, and upon addition of ascorbate, this fraction of the protein undergoes the same spectroscopic changes observed for the fusion protein: H-heme vanishes, and a fraction of the L-heme changes to a second species. The spectrum of the tag-free protein, however, has a significant additional new low-spin heme species (TF-heme) with a g_z = 2.97 signal relative to the MBP fusion protein. This TF-heme also appears to be a bis-His heme based on the *g* values (with crystal field parameters that make distinguishing between neutral His and imidazolate character ambiguous). The amount of TF-heme is approximately equal to that of the normal heme species, which suggests that approximately one-half of the protein is in this other state. The addition of ascorbate to the tag-free protein had no effect on the state ascribed to the TF-heme, suggesting that it cannot be reduced by ascorbate.

The molecular basis of the generation of the new TF-heme state is unclear at this time, and because the visible absorbance spectra of the tag-free enzyme are nearly identical to those of the MBP fusion, it is presumed that the generation of the TF-heme state may be reversible at room temperature. However, these data do imply that there are inherent differences in conformational flexibility in the MBP-tagged and tag-free forms of the *So* CcP enzyme, consistent with the differences seen in the kinetics of peroxide turnover and activation rate in the two forms of the enzyme.

Catalytic Behavior of *So* CcP. We monitored the kinetic parameters of peroxide turnover and activation of *So* CcP in the presence of several electron donor proteins as well as MBP-tagged and tag-free versions of the enzyme. It is clear that the kinetic behavior of the MBP-tagged protein differs substantially from that of the tag-free protein; without the MBP tag, *So* cytochrome c_5 gives the fastest peroxide turnover, whereas the MBP-tagged protein is most active when horse heart cytochrome *c* or azurin is used as the electron donor. These data indicate that the relatively large MBP protein has a principle effect on the binding of electron donors.

It is surprising that the peroxide turnover rates of the oxidized protein never reach the rates of the semireduced proteins. This may indicate that there is a slow step in reductive activation that is required for maximal turnover efficiency and is not attained during the time course of the in vitro experiments. This is supported by the observation that peroxide binding (K_m) differs between oxidized and semireduced *So* CcP. The slow time-dependent decay of the activated protein, which was required for an optimal fit of the computation model to the lag-phase data, may also contribute to the rate differences. One possible explanation for this deactivation is dissociation of the dimeric *So* CcP at the low nanomolar concentrations in the in vitro assay.[14]

The catalytic parameters we report for peroxide turnover of *So* CcP in the presence of various electron donors are in the

Table 5. Kinetic Parameters of the Oxidized and Semireduced States of Tag-Free *So* CcP Variants using *So* Cytochrome c_5 as the Electron Donor

			K_m for H_2O_2 (μM)	k_{cat}^{obs} (s^{-1})	k_{act} (s^{-1})	k_1 (s^{-1})[a]
loop 1	P75T/H81K/E84Q	oxidized	1.0 ± 0.3	0.3 ± 0.1	0.6 ± 0.2	0.56 ± 0.04
		semireduced	0.4 ± 0.3	13 ± 1	na[b]	na[b]
loop 3	M219Q/F247N	oxidized	1.6 ± 0.2	0.5 ± 0.1	0.09 ± 0.01	0.60 ± 0.04
		semireduced	0.5 ± 0.3	5.9 ± 0.5	na[b]	na[b]
wild type		oxidized	0.6 ± 0.5	7 ± 5	0.07 ± 0.02	7 ± 1
		semireduced	0.3 ± 0.1	73 ± 5	na[b]	na[b]

[a]Turnover values correspond to 4 μM electron donor. [b]Not available.

same range as those reported for other BCcPs elsewhere in the literature. *So* CcP binds peroxide much more tightly, as assayed by K_m values, than other representative BCcPs. This may reflect a difference in the peroxide sensitivity of components of the *Shewanella* periplasm when compared with those of other Gram-negative bacteria. The values of k_{cat}^{obs} listed in Table 3 are not the maximal values for the BCcP enzymes; maximal peroxide turnover, in the presence of a saturating level of electron donor, will be several times higher. Given the reported concentrations of *So* cytochrome c_5 isolated from cells grown under low-oxygen conditions (34 μmol of cytochrome c_5/kg of cell pellet[36]), we estimate that the in vivo concentration of *So* cytochrome c_5 in the periplasm is on the order of 300 μM, suggesting that in vivo rates of peroxide turnover will be much faster than those reported here. We observed that the relationship between peroxide concentration and electron donor concentration was linear up to a cytochrome c_5 concentration of 40 μM (data not shown).

Studies with other BCcPs have demonstrated that a variety of small proteins can act as electron donors, and that the peroxide turnover rate of the BCcP depends on the identity of the electron donor.[37] This variability is attributed to differences in the binding orientation of the various electron donors. In the case of *Pd* CcP, computational modeling and NMR identified two possible electron donor binding sites: one that was favored by horse heart cytochrome *c* and a different binding site favored by the native *Pd* electron donor cytochrome c_{550}.[8,9] Our data suggest a similar model for *So* CcP. For *So* CcP, peroxide turnover is most efficient for the tag-free protein when the native electron donor *So* cytochrome c_5 is used, suggesting that *So* cytochrome c_5 binds to the *So* CcP surface in a unique mode that is optimized for electron transfer. The lower turnover rates for non-native electron donors may result from weaker binding to the *So* CcP surface, or in a slightly different orientation that is less optimal for electron transfer. Moreover, we show that the presence of the MBP tag favors the turnover of peroxide in the presence of the non-native electron donors azurin and horse heart cytochrome *c*. This suggests that the bulky MBP protein either increases the binding affinity of non-native electron donors or forces the non-native electron donor to bind in a mode that facilitates more rapid electron transfer.

Previous studies of BCcP family members and electron donor proteins have suggested that the electrostatic potential of the protein surfaces allows the native electron donor to select a proper binding site. *So* cytochrome c_5 has an equal number of positive and negative amino acids, but the arrangement of positive and negative charges results in a substantial dipole moment (0.56 D/atom).[38] Horse heart cytochrome *c* has an excess of positively charged residues, but the arrangement of charges results in a lower net dipole (0.324 D/atom). This difference in the electrostatic potential of the two electron donors may contribute to the differences in the binding modes. We are currently undertaking biophysical experiments to explore the differences in the equilibrium binding between electron donors and various forms of the *So* CcP protein.

Tag-Free versus MBP Fusion *So* CcP. The *So* CcP protein was expressed in *E. coli* with an N-terminal MBP fusion. This fusion protein system allows purification of the *So* CcP protein in high yield, an important criterion for its use as a model BCcP in biophysical studies. We therefore investigated the potential differences between the *So* CcP−MBP fusion protein and tag-free *So* CcP. Optical spectroscopy failed to show any differences between the heme environment in the fusion protein and the tag-free protein. However, EPR spectroscopy demonstrates that the tag-free protein has greater conformational flexibility than the *So* CcP−MBP fusion protein, as half of the tag-free *So* CcP was trapped in a "TF-heme" state in the low-temperature EPR experiments. The peroxidase turnover data suggest that this additional conformational flexibility facilitates interaction with the native electron donor *So* cytochrome c_5, resulting in higher rates of peroxide turnover. We conclude that the MBP fusion protein affects the conformational flexibility, but not the underlying fold, of the *So* CcP protein, demonstrating that fusion proteins should be employed carefully in biochemical and biophysical studies.

Kinetic Modeling and Comparison to Other BCcPs. Previous reports[39] have investigated the lag-phase behavior of the model BCcP family member from *P. aeruginosa*. The authors noted, as we do in this report, that the lag-phase behavior may result from equilibrium binding between oxidized CcP and a reduced electron donor followed by electron transfer, which can be modeled using an equilibrium binding constant and an activation rate. The authors reported kinetic parameters (K_m = 4 μM, and k_{act} = 0.2 s^{-1})[39] that agree remarkably well with those we have established for *So* CcP. Our use of a modern computational framework in Python and SciPy allows us to quickly extract the activation and peroxidase rates from the kinetic progress curve. The framework we developed has been used here and in continuing experiments to study the differential effects of mutations on the activation or the peroxide turnover rate.

Effect of Activation Loop Mutations on Activation and Peroxide Turnover. There are few reports of mutagenesis studies of BCcP family members. With the exception of the *Geobacter* CcP loop 2 mutation,[18] reports have been limited to mutation of residues with hypothesized roles in heme ligation, proton delivery, or transfer of electrons between the hemes.[40,41] In general, these mutational studies have resulted in complete deactivation of the peroxide turnover activity of the enzyme, and full kinetic characterization has been rarely reported.[40,41] In this study, we focus on mutations in flexible regions that are not specifically implicated in catalysis. These locations can be mapped onto the fully oxidized *Psa* CcP X-ray crystal structure,

as shown in Figure 6, which demonstrates that in the case of the M219Q/F247N double mutation, both positions are well removed from the low-potential catalytic heme.

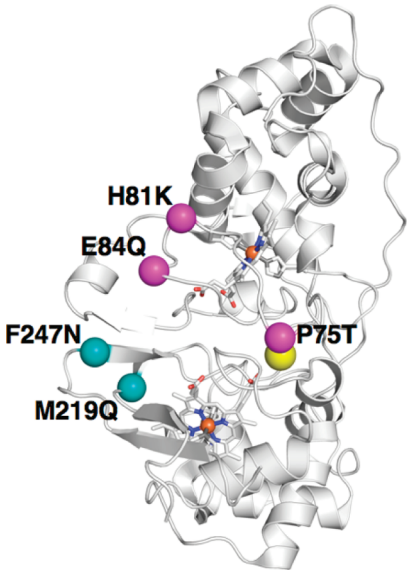

Figure 6. Depiction of the mutations made in either loop 1 or loop 3 in *So* CcP. Using the fully oxidized *Psa* structure as a model, locations of the loop 1 P75T/H81K/E85Q triple mutant are indicated as magenta spheres at the α-carbon positions. The loop 3 M219Q/F247N double mutant positions are shown as teal spheres at the predicted α-carbon positions.

A sequence alignment of *Ne* and *So* CcPs shows extremely strong sequence conservation in several loop regions. On the basis of this sequence conservation and the structural evidence of the importance of these loops in the conformational change required for activation, we predicted that the *So* CcP would not require reductive activation. However, UV−visible spectroscopy, EPR spectroscopy, and peroxide turnover indicate that this is not the case. We therefore sought to introduce mutations into the activation loops of *So* CcP in an attempt to convert *So* CcP into an *Ne*-type BCcP. For the BCcP of *G. sulfurreducens*, the S134P/V135K double mutant transforms the L-loop (loop 1) into an "always open" state, as determined crystallographically.[18] In attempting a similar conversion, we introduced *So* CcP mutations into loop 1 (P75T/H81K/E84Q) and loop 3 (M219Q/F247N). We did not introduce mutations into the loop 2 region because the sequences are already nearly identical between *So* and *Ne* CcPs; the only differences are in positions otherwise conserved between *Psa*- and *Ne*-type BCcPs that are not likely to be important in reductive activation.

We found that neither set of mutations successfully transformed *So* CcP into a constitutive, *Ne*-type BCcP. However, the loop 1 triple mutant (P75T/H81K/E84Q) was activated much more quickly than the wild-type protein during the in vitro peroxidase turnover assay. This suggests that the three simultaneous mutations have successfully modulated the structure of loop 1 to favor the active state. Mutations in the loop regions were accompanied by severe decreases in peroxidase activity for the *So* CcP variants, indicating that the mutations have effects on catalytic activity in addition to changes in the equilibrium between the active and inactive states. Interestingly, the M219Q/F247N double mutation affects catalysis despite its location near the H-heme, far from the catalytic site. This suggests that the M219Q/F247N double mutation also has a subtle impact on the equilibrium between the inactive and active conformations of the protein. Indeed, the EPR characterization of either of the two mutants described here underscores that structural conformations around the H-heme are strongly affected by the sequences of loops 1 and 3. The loop 1 and loop 3 mutants both reveal that multiple heme states can be adopted, while fully oxidized, which presumably negatively impact catalytic competency, and while the tag-free version of the loop 3 M219Q/F247N mutant appears to be similar to the native enzyme, the L-heme clearly displays slight perturbations in *g* values, suggesting that the electronic structure of the L-heme is not truly native-like. Together, these data strongly suggest that all of the flexible loop regions identified in other BCcP family members are also important for redox-coupled conformational changes in the *So* CcP.

CONCLUSIONS

This study describes the recombinant expression and characterization of a BCcP family member, the *So* CcP. UV−visible spectroscopy and EPR spectroscopy confirm the similarity between *So* CcP and other *Psa*-like peroxidases, while EPR also suggests subtle differences in the conformational flexibility of the *So* CcP when compared to other bacterial peroxidases. Peroxide turnover of *So* CcP can be monitored using a variety of native and non-native electron donor proteins, and Michaelis−Menten analysis confirms that *So* CcP catalyzes the turnover of peroxide with catalytic efficiencies similar to those of other documented BCcPs. The *So* CcP can be easily purified in high yield from the *E. coli* system, and sequence variants have proven to be easy to express and purify, making *So* CcP an excellent system for mutational study. We hope that the detailed kinetic characterization we present here can serve to initiate an extensive mechanistic study of the BCcP family and, more broadly, the mechanism of electron transfer in proteins.

ASSOCIATED CONTENT

Supporting Information

Mutagenesis primers, Python code for least-squares fitting of lag-phase kinetic data, SDS−PAGE gel of purification of *So* CcP as an MBP fusion, and EPR data. This material is available free of charge via the Internet at http://pubs.acs.org.

AUTHOR INFORMATION

Corresponding Author

*Department of Chemistry, Boston University, 590 Commonwealth Ave., Boston, MA 02215. Telephone: (617) 358-2816. Fax: (617) 353-6466. E-mail: elliott@bu.edu.

Author Contributions

G.S.P. and K.E.F. contributed equally to this work.

Funding

This work was supported by National Institutes of Health Grant R01-GM072663 and the Boston University Undergraduate Research Opportunities Program.

Notes

The authors declare no competing financial interest.

ACKNOWLEDGMENTS

We thank Drs. Frank Collart and Yuri Londer (Argonne National Laboratory), Michele McGuirl (University of Montana), and Mr. Ben Levin for their kind supply of reagents used in this work.

■ ABBREVIATIONS

CcP, cytochrome *c* peroxidase; BCcP, bacterial cytochrome *c* peroxidase; MBP, maltose binding protein; HRP, horseradish peroxidase; *Psa*, *P. aeruginosa*; *So*, *S. oneidensis*; *Gs*, *G. sulfurreducens*; *Ne*, *N. europaea*; *Rc*, *R. capsulatus*; *Pd*, *Pa. denitrificans*; *Pss*, *P. stutzeri*; *Psn*, *P. nautica*; *Mc*, *M. casulatus* (Bath); NHE, normal hydrogen electrode; EPR, electron paramagnetic resonance; S-100, Sepharcryl 100.

■ REFERENCES

(1) Chandel, N. S., McClintock, D. S., Feliciano, C. E., Wood, T. M., Melendez, J. A., Rodriguez, A. M., and Schumacker, P. T. (2000) Reactive oxygen species generated at mitochondrial complex III stabilize hypoxia-inducible factor-1α during hypoxia: A mechanism of O_2 sensing. *J. Biol. Chem. 275*, 25130−25138.

(2) Halliwell, B., and Gutteridge, J. M. C. (1992) Biologically relevant metal ion-dependent hydroxyl radical generation. An update. *FEBS Lett. 307*, 108−112.

(3) Van Spanning, R. J., De Boer, A. P., Reijnders, W. N., Westerhoff, H. V., Stouthamer, A. H., and Van Der Oost, J. (1997) FnrP and NNR of *Paracoccus denitrificans* are both members of the FNR family of transcriptional activators but have distinct roles in respiratory adaptation in response to oxygen limitation. *Mol. Microbiol. 23*, 893−907.

(4) Hiner, A., Raven, E. L., Thorneley, R., Garcia-Canovas, F., and Rodriguez-Lopez, J. N. (2002) Mechanisms of compound I formation in heme peroxidases. *J. Inorg. Biochem. 91*, 27−34.

(5) Finzel, B. C., Poulos, T. L., and Kraut, J. (1984) Crystal structure of yeast cytochrome c peroxidase refined at 1.7-Å resolution. *J. Biol. Chem. 259*, 13027−13036.

(6) Ellfolk, N., Ronnberg, M., Aasa, R., Andreasson, L. E., and Vanngard, T. (1983) Properties and function of the two hemes in *Pseudomonas* cytochrome c peroxidase. *Biochim. Biophys. Acta 743*, 23−30.

(7) Pettigrew, G. W., Echalier, A., and Pauleta, S. R. (2006) Structure and mechanism in the bacterial dihaem cytochrome c peroxidases. *J. Inorg. Biochem. 100*, 551−567.

(8) Pettigrew, G. W., Prazeres, S., Costa, C., Palma, N., Krippahl, L., Moura, I., and Moura, J. J. (1999) The structure of an electron transfer complex containing a cytochrome c and a peroxidase. *J. Biol. Chem. 274*, 11383−11389.

(9) Pettigrew, G. W., Pauleta, S. R., Goodhew, C. F., Cooper, A., Nutley, M., Jumel, K., Harding, S. E., Costa, C., Krippahl, L., Moura, I., and Moura, J. (2003) Electron transfer complexes of cytochrome c peroxidase from *Paracoccus denitrificans* containing more than one cytochrome. *Biochemistry 42*, 11968−11981.

(10) Ronnberg, M., and Ellfolk, N. (1978) *Pseudomonas* cytochrome c peroxidase. Initial delay of the peroxidatic reaction. Electron transfer properties. *Biochim. Biophys. Acta 504*, 60−66.

(11) Echalier, A., Goodhew, C. F., Pettigrew, G. W., and Fulop, V. (2006) Activation and catalysis of the di-heme cytochrome c peroxidase from *Paracoccus pantotrophus*. *Structure 14*, 107−117.

(12) Echalier, A., Brittain, T., Wright, J., Boycheva, S., Mortuza, G. B., Fulop, V., and Watmough, N. J. (2008) Redox-linked structural changes associated with the formation of a catalytically competent form of the diheme cytochrome c peroxidase from *Pseudomonas aeruginosa*. *Biochemistry 47*, 1947−1956.

(13) Shimizu, H., Schuller, D. J., Lanzilotta, W. N., Sundaramoorthy, M., Arciero, D. M., Hooper, A. B., and Poulos, T. L. (2001) Crystal structure of *Nitrosomonas europaea* cytochrome c peroxidase and the structural basis for ligand switching in bacterial di-heme peroxidases. *Biochemistry 40*, 13483−13490.

(14) Gilmour, R., Goodhew, C. F., Pettigrew, G. W., Prazeres, S., Moura, J. J. G., and Moura, I. (1994) The kinetics of the oxidation of cytochrome c by *Paracoccus* cytochrome c peroxidase. *Biochem. J. 300*, 907−914.

(15) Alves, T., Besson, S., Duarte, L. C., Pettigrew, G. W., Girio, F., Devreese, B., Vandenberghe, I., Van Beeumen, J. J., Fauque, G., and Moura, I. (1999) A cytochrome c peroxidase from *Pseudomonas nautica* 617 active at high ionic strength: Expression, purification and characterization. *Biochim. Biophys. Acta 1434*, 248−259.

(16) De Smet, L., Pettigrew, G. W., and Van Beeumen, J. J. (2001) Cloning, overproduction and characterization of cytochrome c peroxidase from the purple phototrophic bacterium *Rhodobacter capsulatus*. *Eur. J. Biochem. 268*, 6559−6568.

(17) Timoteo, C. G., Tavares, P., Goodhew, C. F., Duarte, L. C., Jumel, K., Girio, F. M. F., Harding, S., Pettigrew, G. W., and Moura, I. (2003) Ca^{2+} and the bacterial peroxidases: The cytochrome c peroxidase from *Pseudomonas stutzeri*. *J. Biol. Inorg. Chem. 8*, 29−37.

(18) Hoffmann, M., Seidel, J., and Einsle, O. (2009) CcpA from *Geobacter sulfurreducens* is a basic di-heme cytochrome c peroxidase. *J. Mol. Biol. 393*, 951−965.

(19) Arciero, D., and Hooper, A. B. (1994) A di-heme cytochrome c peroxidase from *Nitrosomonas europaea* catalytically active in both the oxidized and half-reduced states. *J. Biol. Chem. 269*, 11878−11886.

(20) Zahn, J. A., Arciero, D. M., Hooper, A. B., Coats, J. R., and DiSpirito, A. A. (1997) Cytochrome c peroxidase from *Methylococcus capsulatus* Bath. *Arch. Microbiol. 168*, 362−372.

(21) Londer, Y. Y., Giuliani, S. E., Peppler, T., and Collart, F. R. (2008) Addressing *Shewanella oneidensis* "cytochromome": The first step towards high-throughput expression of cytochromes c. *Protein Expression Purif. 62*, 128−137.

(22) Arslan, E., Schulz, H., Zufferey, R., Kunzler, P., and Thony-Meyer, L. (1998) Overproduction of the *Bradyrhizobium japonicum* c-type cytochrome subunits of the cbb3 oxidase in *Escherichia coli*. *Biochem. Biophys. Res. Commun. 251*, 744−747.

(23) Van Gelder, B., and Slater, E. C. (1962) The extinction coefficient of cytochrome c. *Biochim. Biophys. Acta 58*, 593−595.

(24) Soininen, R., and Ellfolk, N. (1972) *Pseudomonas* cytochrome c peroxidase. IV. Some kinetic properties of the peroxidations reaction, and enzymatic determination of the extinction coefficients of *Pseudomonas* cytochrome c-551 and azurin. *Acta Chem. Scand. 26*, 861−872.

(25) Mason, A. B., He, Q. Y., Halbrooks, P. J., Everse, S. J., Gumerov, D. R., Kaltashov, I. A., Smith, V. C., Hewitt, J., and MacGillivray, R. T. A. (2002) Differential effect of a his tag at the N- and C-termini: Functional studies with recombinant human serum transferrin. *Biochemistry 41*, 9448−9454.

(26) Song, J., and Markley, J. L. (2007) Cautionary tail: The presence of an N-terminal tag on dynein light-chain Roadblock/LC7 affects its interaction with a functional partner. *Protein Pept. Lett. 14*, 265−268.

(27) Goodhew, C. F., Wilson, I. B., Hunter, D. J., and Pettigrew, G. W. (1990) The cellular location and specificity of bacterial cytochrome c peroxidases. *Biochem. J. 271*, 707−712.

(28) Gilmour, R., Prazeres, S., McGinnity, D. F., Goodhew, C. F., Moura, J. J., Moura, I., and Pettigrew, G. W. (1995) The affinity and specificity of Ca^{2+}-binding sites of cytochrome-c peroxidase from *Paracoccus denitrificans*. *Eur. J. Biochem. 234*, 878−886.

(29) Gilmour, R., Goodhew, C. F., Pettigrew, G. W., Prazeres, S., Moura, I., and Moura, J. J. (1993) Spectroscopic characterization of cytochrome c peroxidase from *Paracoccus denitrificans*. *Biochem. J. 294*, 745−752.

(30) Foote, N., Peterson, J., Gadsby, P., Greenwood, C., and Thomson, A. (1985) Redox-linked spin-state changes in the di-haem cytochrome c-551 peroxidase from *Pseudomonas aeruginosa*. *Biochem. J. 230*, 227−237.

(31) Prazeres, S., Moura, J. J., Moura, I., Gilmour, R., Goodhew, C. F., Pettigrew, G. W., Ravi, N., and Huynh, B. H. (1995) Mossbauer characterization of *Paracoccus denitrificans* cytochrome c peroxidase. Further evidence for redox and calcium binding-induced heme-heme interaction. *J. Biol. Chem. 270*, 24264−24269.

(32) Aasa, R., Ellfolk, N., Ronnberg, M., and Vanngard, T. (1981) Electron paramagnetic resonance studies of *Pseudomonas* cytochrome c peroxidase. *Biochim. Biophys. Acta 670*, 170−175.

(33) Foote, N., Peterson, J., Gadsby, P. M., Greenwood, C., and Thomson, A. J. (1984) A study of the oxidized form of *Pseudomonas*

aeruginosa cytochrome c-551 peroxidase with the use of magnetic circular dichroism. *Biochem. J. 223*, 369−378.
(34) Hu, W., De Smet, L., Van Driessche, G., Bartsch, R. G., Meyer, T. E., Cusanovich, M. A., and Van Beeumen, J. (1998) Characterization of cytochrome c-556 from the purple phototrophic bacterium *Rhodobacter capsulatus* as a cytochrome-c peroxidase. *Eur. J. Biochem. 258*, 29−36.
(35) Taylor, C. (1977) The EPR of low spin heme complexes: Relation of the tau2g hole model to the directional properties of the g tensor, and a new method for calculating the ligand field parameters. *Biochim. Biophys. Acta 491*, 137−148.
(36) Meyer, T. E., Tsapin, A. I., Vandenberghe, I., DeSmet, L., Frishman, D., Nealson, K. H., Cusanovich, M. A., and vanBeeumen, J. J. (2004) Identification of 42 possible cytochrome c genes in the *Shewanella oneidensis* genome and characterization of six soluble cytochromes. *OMICS 8*, 57−77.
(37) Pauleta, S. R., Cooper, A., Nutley, M., Errington, N., Harding, S., Guerlesquin, F., Goodhew, C. F., Moura, I., Moura, J. J. G., and Pettigrew, G. W. (2004) A copper protein and a cytochrome bind at the same site on bacterial cytochrome c peroxidase. *Biochemistry 43*, 14566−14576.
(38) Felder, C. E., Prilusky, J., Silman, I., and Sussman, J. L. (2007) A server and database for dipole moments of proteins. *Nucleic Acids Res. 35*, W512−W521.
(39) Foote, N., Turner, R., Brittain, T., and Greenwood, C. (1992) A quantitative model for the mechanism of action of the cytochrome c peroxidase of *Pseudomonas aeruginosa*. *Biochem. J. 283*, 839−843.
(40) De Smet, L., Savvides, S. N., Van Horen, E., Pettigrew, G., and Van Beeumen, J. J. (2006) Structural and mutagenesis studies on the cytochrome c peroxidase from *Rhodobacter capsulatus* provide new insights into structure-function relationships of bacterial di-heme peroxidases. *J. Biol. Chem. 281*, 4371−4379.
(41) Hsiao, H.-C., Boycheva, S., Watmough, N. J., and Brittain, T. (2007) Activation of the cytochrome c peroxidase of *Pseudomonas aeruginosa*. The role of a heme-linked protein loop: A mutagenesis study. *J. Biol. Inorg. Chem. 101*, 1133−1139.
(42) Schütz, B., Seidel, J., Sturm, G., Einsle, O., and Gescher, J. (2011) Investigation of the Electron Transport Chain to and the Catalytic Activity of the Diheme Cytochrome c Peroxidase CcpA of *Shewanella oneidensis*. *Appl. Environ. Microbiol. 77*, 6172−6180.